

Supercooled water and the kinetic glass transition

F. Sciortino,¹ P. Gallo,² P. Tartaglia,¹ and S.-H. Chen²

¹*Dipartimento di Fisica and Istituto Nazionale per la Fisica della Materia, Università di Roma La Sapienza, Piazza le Aldo Moro 2, I-00185, Roma, Italy*

²*Department of Nuclear Engineering, Massachusetts Institute of Technology, Cambridge, Massachusetts 02139*

(Received 8 May 1996)

We present a molecular-dynamics study of the self-dynamics of water molecules in deeply supercooled liquid states. We find that the decay of single-particle dynamics correlation functions is characterized by a fast initial relaxation toward a plateau and by a region of self-similar dynamics, followed at late times by a stretched exponential decay. We interpret such results in the framework of the mode-coupling theory for supercooled liquids. We relate the apparent anomalies of the transport coefficients in water on lowering the temperature to the formation of cages and to the associated slow dynamics resulting from the presence of long-lived molecular cages. The so-called critical Angell temperature in supercooled water could thus be interpreted as kinetic glass transition temperature, relaxing the need of a thermodynamic singularity for the explanation of the anomalies of liquid water. [S1063-651X(96)09512-8]

PACS number(s): 61.20.Ja, 64.70.Pf

I. INTRODUCTION

The behavior of liquid water on supercooling has been the subject of a long-standing scientific debate for the past 30 years [1–3]. It has been found that there are anomalous increases of thermodynamic quantities and apparent divergences of dynamic quantities on approaching a singular but experimentally unaccessible temperature T_s of about 227 K at ambient pressure. This discovery has stimulated an enormous amount of experimental, theoretical, and computational work in an attempt to clarify the origin of the singularity. A recent detailed review of all these works can be found in Ref. [3].

In the past five years, efforts have been directed at elucidating possible thermodynamic scenarios compatible with the trend of experimental data. The pronounced increases in isothermal compressibility, isobaric heat capacity, and the change of sign of the thermal expansion coefficient of liquid water upon supercooling can result from three possible causes: (i) the existence of a continuous, retracing spinodal curve bounding the superheated, stretched, and supercooled states of liquid water [4–6]; (ii) the existence of a metastable, low-temperature critical point [6,7]; or (iii) the progressive increase of four hydrogen-bonded (HB) coordinated water molecules, favorable in terms of the low energy of this state, but unfavorable in terms of the high local volume and the low orientational entropy [8,9].

While the phase behavior of supercooled water has been debated extensively, not much attention has been devoted so far to dynamics near the apparent singular temperature. Computation of long-time behavior of dynamical quantities could be very valuable. Therefore, it is timely to make an effort in the direction of understanding the origin of the apparent divergences of transport coefficients in water on supercooling. In particular, if the dynamics could be rationalized without resorting to an underlying thermodynamics singularity, then the possibility of a singularity-free picture capable of explaining satisfactorily the behavior of thermodynamic quantities would be reinforced [9].

Already in the late 1980s, Prielmeier *et al.* [10], based on NMR measurements and fitting of the self-diffusion constant in supercooled water, and Angell [11] commented on the possible relationship between the power-law temperature dependence of transport coefficients in water and the predictions of mode-coupling theory (MCT) [12] for the glass transition in supercooled liquids. More recently, the translational region of Raman spectra of water has been interpreted in terms of scaling behavior predicted by MCT [13]. Today, due to the availability of sufficient computational power and the extensive development of MCT [14], such suggestions as to the connection between the existence of a kinetic glass transition temperature and the divergence of the transport coefficients in water can be carefully examined.

In this paper we aim to test MCT predictions for the correlation functions of single-particle dynamics in water with corresponding quantities calculated from molecular-dynamics (MD) simulations, carried out for sufficiently long time as to allow the slow dynamics to be observed. In doing so, we try to assess to what extent the MCT, which has been shown to describe simple liquids [15,16], is applicable also to the description of the single-particle dynamics of supercooled water, a hydrogen bonded liquid with strong nonisotropic interactions among molecules. A brief report in this direction has already been published [17].

The paper is organized as follows. In Sec. II we briefly recall the predictions of MCT. In Sec. III we discuss in detail the MD simulations performed and the potential used. Section IV is divided into subsections where we present the numerical results for correlation functions in time domains and we discuss the rotational motion. Specifically, we compute and compare the results of the mean-squared displacement, the Van Hove space-time self-correlation function, the intermediate scattering function, and the angular correlations. In Sec. V we summarize our conclusions.

II. MODE-COUPLED THEORY FOR SUPERCOOLED LIQUIDS

In this section we summarize the predictions of MCT relevant for interpreting our MD simulation data. Our discus-

sion emphasizes the results of the so-called idealized MCT [14], in which hopping effects are neglected. In contrast to the MCT for critical phenomena [18], the emphasis of the MCT theory for the supercooled dense liquids is on distances comparable to the interparticle distance, or in Fourier space, for Q vectors close to the first maximum Q_{\max} of the structure factor $S(Q)$. Therefore, the Q dependence of the dynamics quantities around Q_{\max} is of interest.

MCT for supercooled liquids is a theory that takes into account the cage effect [19], which is associated with a transient trapping of molecules on lowering the temperature or on increasing the density. The microscopic density fluctuations of locally disordered high-temperature and low-density fluids tend to relax rapidly on the time scale of a few picoseconds. Upon lowering the temperature or increasing the density of the liquid, there is a rapid increase in the local order surrounding the particle, leading to a substantial increase of the structural relaxation time. In the supercooled or dense liquid regime a trapped particle in a cage can migrate only through rearrangement of a large number of particle surrounding it. In this sense there is a strong coupling between the single-particle motion and the density fluctuations of the fluid. According to MCT, static density fluctuations [i.e., $S(Q)$] completely determine the long-time dynamical behavior.

MCT predicts the evolution of any correlator that has a nonzero overlap with density [20], such as, e.g., the density itself, the current density, and the tagged particle density. In the following we will denote such a generic correlator as $\phi_Q(t)$. The evolution of $\phi_Q(t)$ is controlled by a retarded memory function, a nonlinear functional of the density. The idealized MCT predicts that on moving along a path in the pressure-temperature plane, a line $T_c(P)$ is crossed on which $\phi_Q(\infty)$ no longer decays to zero. Such a line defines the locus of the ideal ergodic to nonergodic transition. This line separates the liquid and the glass regions. On the liquid side, the system is ergodic and $\lim_{t \rightarrow \infty} \phi_Q(t) = 0$. Close to the line, on the liquid side, $\phi_Q(t)$ has a two step relaxation behavior displaying a fast and a slow decay. The two relaxation times become more and more separated on a time scale on approaching the line. When the fast process decays, $\phi_Q(t)$ reaches a plateau value f_Q^c the so-called nonergodicity parameter. Only after the second relaxation is completed, $\phi_Q(t)$ relaxes to zero. The time interval in which the correlation function is close to the plateau f_Q^c is called the β -relaxation region, while the long-time region is called the α -relaxation region. The β -relaxation region is centered around a time t_σ , which increases on decreasing the distance σ from the critical line in the pressure-temperature plane. In particular, approaching the ideal glass transition line along an isobaric path, using the temperature as an external driving parameter, the distance σ can be measured by $T - T_c(P)$.

The idealized MCT predicts the dependence on σ of t_σ and the functional form of the decay of $\phi_Q(t)$ in the β -relaxation region. It states that (i) t_σ scales in $|\sigma|$ as

$$t_\sigma = t_0 |\sigma|^{-1/2a}, \quad (1)$$

where t_0 is a characteristic microscopic time; (ii) the approach to the plateau is described, in leading order in time, by a power law with exponent a ,

$$\phi_Q(t) - f_Q^c = B_Q |\sigma|^{1/2} (t/t_\sigma)^a = B_Q (t/t_0)^{-a}; \quad (2)$$

and (iii) on the liquid side of the phase diagram, $\phi_Q(t)$ departs from the plateau value f_Q^c as a power law with exponent b ,

$$\phi_Q(t) - f_Q^c = -C_Q |\sigma|^{1/2} (t/t_\sigma)^b = -C_Q (t/\tau)^b, \quad (3)$$

where

$$\tau = t_0 |\sigma|^{-(1/2b + 1/2a)}. \quad (4)$$

Expression (3) is the leading term in the expansion in powers of t^b . The leading term [Eq. (3)] is often called the von Schweidler law and its region of validity is often rather limited [21].

The constants f_Q^c , B_Q , and C_Q in Eqs. (2) and (3) are T independent, while the exponents a and b are T and Q independent. In real space, Eqs. (2) and (3) express the predictions of a separation of space and time. Any space-dependent correlation function $\phi(r, t)$ in the β region can be expressed as

$$\phi(r, t) = F(r) + H(r)G(t), \quad (5)$$

where $G(t)$ is proportional to t^{-a} or t^b , depending on the time scale, and $F(r)$ and $H(r)$ are related to the Fourier transform of f_Q^c , and B_Q or C_Q , respectively.

The exponents a and b are connected and both depend on the specific point on the transition line crossed on moving the system along the P - T plane. For example, cooling the system along different isobars will produce crossing of the transition line in different points, which will in the end imply different values for the a and b exponents. a can be related to b by the transcendental equation

$$\frac{[\Gamma(1-a)]^2}{\Gamma(1-2a)} = \frac{[\Gamma(1+b)]^2}{\Gamma(1+2b)}, \quad (6)$$

where Γ is the gamma function and $0 < a \leq 0.5$ and $0 < b \leq 1$.

Equation (3) describes the region where $\phi_Q(t) - f_Q^c$ is small. It states that curves for different values of σ can be scaled onto a single master curve if plotted as a function of t/τ . MCT predicts that the dependence of ϕ_Q on the scaled time t/τ is valid also in the α -relaxation regime. In other words, $\phi_Q(t)$ does not depend on T and P explicitly, but only via the P and T dependence of τ . Thus one single master curve describes entirely the α -relaxation regime. It has been shown numerically that the shape of the master curve in the α region is, within MCT, well represented by a stretched exponential form $e^{-(t/\tau)^\beta}$. τ plays the role of relevant time in the system and diverges [see Eq. (4)] on approaching the transition line with a power γ ,

$$\gamma = \frac{1}{2a} + \frac{1}{2b}. \quad (7)$$

All characteristic times in the system are predicted to be proportional to τ . Thus MCT predicts that the inverse diffusion coefficient D^{-1} diverges as $|\sigma|^{-\gamma}$.

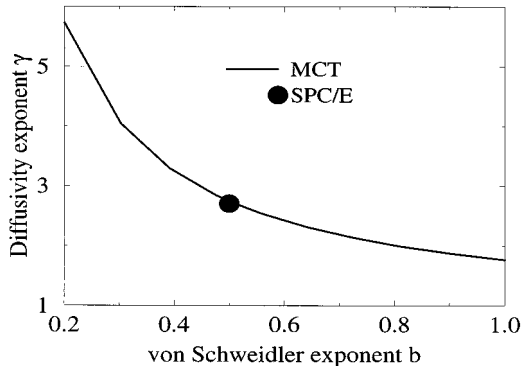


FIG. 1. Full line, relation between the diffusivity exponent γ and the von Schweidler exponent b [Eq. (3)] according to MCT [14]; filled circle, estimated (γ, b) point for SPC/E water along the studied isobar.

We note in passing that Eqs. (6) and (7) relate the exponents a , b , and γ . Thus only one of these three exponent is truly independent. In contrast to critical phenomena, the values of a , b , or γ are not universal and depend on the specific point of the transition line approached, i.e., on $T_c(P)$. In particular, along an isobaric path, D goes like $(T - T_c)^\gamma$. Figure 1 shows the dependence of γ on b as predicted by MCT.

The idealized version of MCT deals with nonlinear interactions of density fluctuations leading to a cage effect with a tendency to produce an ideal glass state and results in a static random configuration. The ideal MCT theory can be formally extended to include also interactions between density fluctuations and currents, leading to relaxation via phonon-assisted hopping, i.e., via jumps over almost static potential barriers [22]. The so-called hopping effects smear out the ideal glass transition and allow for relaxation of density fluctuations below the ideal glass line. Under certain conditions, the relaxation times cross from a power-law behavior to an activated Arrhenius behavior. As we show in the following, hopping effects are not observed in our simulations even at the lowest temperature, suggesting that it is appropriate to compare the low- T dynamics of our system with the idealized version of MCT.

In this paper we focus on the comparison between our MD data and MCT. For this reason we do not compare our data with other (more heuristic) theories for supercooled liquids based on assumptions on the microscopic self-molecule dynamics, such as the so-called trapping model [23]. We only note that an ideal kinetic glass transition is also predicted by this theory [24].

III. COMPUTER SIMULATIONS

We have studied a system composed by 216 water molecules at constant volume. The effective potential used is the *extended simple point charge* SPC/E model [25]. This potential treats a single water molecule as a rigid set of point masses with an OH distance of 0.1 nm and an HOH angle equal to the tetrahedral angle 109.47° . The Coulomb charges are placed on the atoms and their magnitudes are $q_H = 0.4238$ times the electron charge and $q_O = -2q_H$. Oxygen atoms interact via a Lennard-Jones potential, with the

values of $\sigma = 0.31656$ nm and $\epsilon = 0.65017$ kJ mol $^{-1}$. The interaction between pairs of molecules is calculated explicitly when their separation is less than a cutoff distance r_c of 2.5σ . The contribution due to Coulomb interactions beyond r_c is calculated using the reaction-field method, as described by Steinhauser [26]. Also, the contribution of Lennard-Jones interactions between pairs separated more than r_c is included in the evaluation of thermodynamic properties by assuming a uniform density beyond r_c . The MD code used here to calculate the SPC/E trajectories is the same as that used in Ref. [27], where further details are given. A heat bath has been used to allow for heat exchange [28]. In our simulation periodic boundary conditions are used. The time step for the integration of the molecular trajectories is 1 fs. Simulations at low T have been started from equilibrated configurations at higher T . Equilibration has been monitored via the time dependence of the potential energy. In all cases the equilibration time t_{eq} was longer than the time needed to enter in the diffusive regime (see Fig. 8), i.e., $\langle r^2(t_{eq}) \rangle$ larger than 0.1 nm 2 .

The SPC/E potential has been explicitly parametrized to reproduce also the experimental value of the self-diffusion constant at ambient temperature and density 1 g/cm 3 , and it has been widely studied in recent years [29,30]. Moreover, this potential is able to reproduce a pressure-dependent temperature of maximum density (TMD) [7,27,30]. As shown in Ref. [30] the SPC/E 1-bar isobar is characterized by a TMD of 235 K and a corresponding density of 1.026 g/cm 3 . The -40 -MPa isobar is instead characterized by a TMD of about 250 K and a corresponding density of 1.000 g/cm 3 [27], in agreement with the experimental pressure dependence of the TMD line. We have studied the -80 -MPa isobar. Seven simulations have been performed at the state points indicated in Table I, ranging from 35° above the TMD to 45° below, thus covering both the normal and supercooled states of water, for time periods ranging from a few hundred picoseconds at high T to 50 ns at the lowest T .

Densities have been chosen on the basis of trial and error preliminary runs. The corresponding pressures for the chosen final densities are reported in Table I. We have preferred to work at constant volume to avoid the interference of the dynamics of the pressure bath with the dynamics of the system. Note also that the density dependence of the diffusion coefficient over the small range of densities studied (0.966 – 0.990 g/cm 3) is much smaller than the temperature dependence [31,32].

We also present the results of a simulation carried out for hexagonal ice at the temperature of $T = 194$ K with proton disorder. We studied a box of $2.7 \times 2.3 \times 2.2$ nm 3 containing 432 water molecules interacting via the same ESPC potential used for the simulations of liquid water. We simulated a state point laying along the same isobar studied for liquid water, corresponding to a density of 0.9364 g/cm 3 , an average potential energy of the system of -56.2 kJ/mol, and a pressure of -77.7 MPa.

IV. RESULTS

In this section we present the result of our simulations. The discussion is divided into six subsections, from A to E.

TABLE I. Simulated state points.

T (K)	ρ_s (g/cm ³)	E (kJ/mol)	P (MPa)	D (10^{-5} cm ² /s)
284.5	0.984	-48.1	-73 ± 11	$(1.3 \pm 0.1) \times 10^0$
258.5	0.986	-50.0	-76 ± 12	$(5.2 \pm 0.5) \times 10^{-1}$
238.2	0.987	-51.6	-80 ± 10	$(1.4 \pm 0.1) \times 10^{-1}$
224.0	0.984	-52.6	-75 ± 15	$(4.4 \pm 0.4) \times 10^{-2}$
213.6	0.977	-53.4	-78 ± 14	$(1.1 \pm 0.4) \times 10^{-2}$
209.3	0.970	-53.8	-99 ± 18	$(5.1 \pm 0.9) \times 10^{-3}$
206.3	0.966	-54.2	-90 ± 23	$(1.8 \pm 1.1) \times 10^{-3}$

A. Static quantities

In order to define the thermodynamic states covered in our simulation we begin by tabulating the temperature dependence of the density, potential energy, and pressure in Fig. 2. We note that the TMD is around 240 ± 5 K for the ESPC model along this isobar. In order to compare the simulation result with some real experiments in the future we use the TMD as a convenient reference point to measure the temperature distance. From Fig. 2 we note that the energy does not show any significant change of slope at small T , consistently with the fact that all simulations are equilibrated. The pressure of our simulations is constant within the error bar.

Oxygen-oxygen radial distribution functions $g(r)$ for some selected temperatures are shown in Fig. 3. The figure shows that on cooling the system, the first peak of $g(r)$ increases, the first minimum decreases, and the second peak also increases. This illustrates the fact that the nearest- and next-nearest-neighbor shells become more and more well defined. The number of nearest neighbors, calculated by integrating $g(r)$ up to the position of the first minimum (0.32 nm), decreases from 4.2 at high T to almost 4 at the lowest temperature, supporting the progressive formation of a tetrahedral structure around each molecule. Still, the presence of a non-negligible population around 0.35 nm is indicative of the presence of five (or more) coordinated molecules, whose role in the dynamical restructuring of the HB network has been studied previously [31].

The T dependence of the oxygen-oxygen partial structure factor $S_{OO}(Q)$ is shown in Fig. 4. The typical splitted first peak of water, observed via x-ray experiments [33], is recovered. As for $g(r)$, the peak height increases and peaks become better resolved. From Figs. 3 and 4 we see that no dramatic changes in structure happen on cooling the system; no sign of small wave-vector (critical) density fluctuations is observed, in agreement with previous simulations and with the basic idea of MCT. We note also that the position of the maximum Q_{\max} of $S_{OO}(Q)$ does not change significantly with T . Since the T dependence of Q_{\max} is weak, we neglect it in the following and will compare data at different T at the same value of $Q_{\max} = 18 \text{ nm}^{-1}$.

B. Van Hove space-time self-correlation function

Self-dynamics may be studied in greater detail by computing the space-time Van Hove self-correlation function $G_s(r, t)$, which describes the evolution of a test particle from an origin. For a system of N molecules $G_s(r, t)$ is defined as

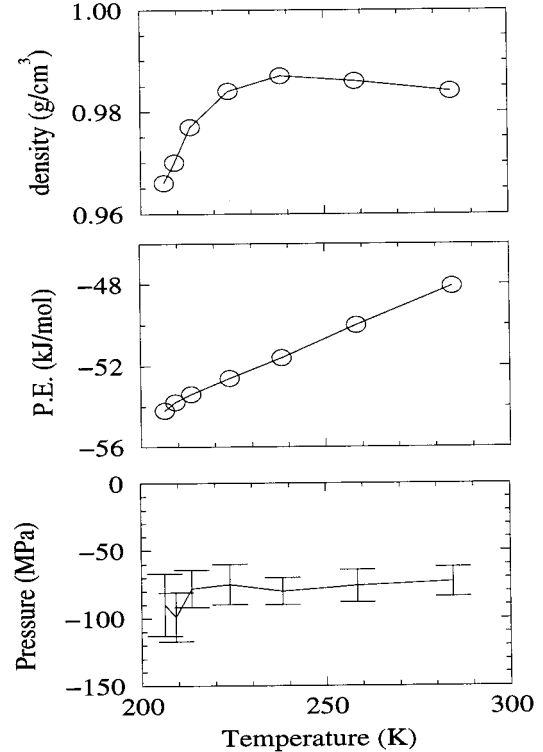


FIG. 2. Temperature dependence of the density (top), potential energy (PE) (center), and pressure (bottom).

$$G_s(\mathbf{r}, t) = \frac{1}{N} \left\langle \sum_{i=1}^N \delta(\mathbf{r} + \mathbf{r}_i(0) - \mathbf{r}_i(t)) \right\rangle. \quad (8)$$

The precise physical interpretation of the Van Hove correlation function is that $4\pi r^2 G_s(r, t) dr$ is the probability of finding a test particle at distance r from the origin at time t given that the same particle was at the origin at time $t=0$. In Figs. 5(a)–5(c) we show $4\pi r^2 G_s(r, t)$ at the lowest T for three selected groups of times. For $t < 0.25$ ps, the ballistic regime [Fig. 5(a)], $G_s(r, t)$ changes rapidly in time. Molecules explore more and more space as the time increases, as shown by the progressive extension of the tails of $G_s(r, t)$. For times approximately between 0.25 and 130 ps, the cage

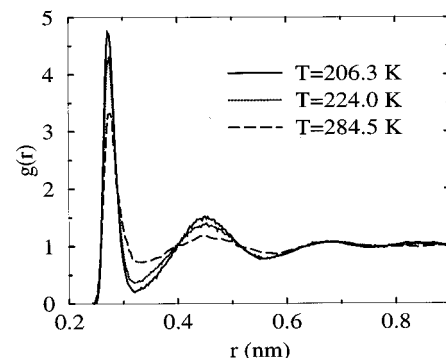


FIG. 3. Radial distribution function $g(r)$ for the oxygen for three selected temperatures.

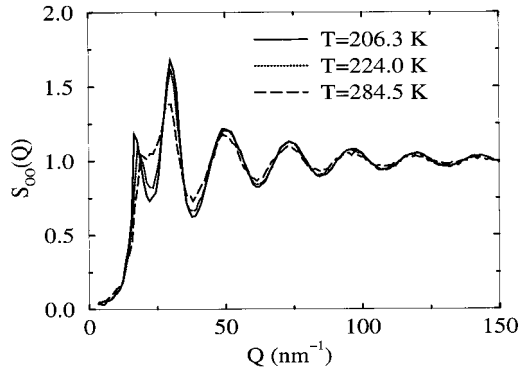


FIG. 4. Structure factor $S_{00}(Q)$ for the oxygen for three selected temperatures.

regime [Fig. 5(b)], $G_s(r,t)$ changes very slowly in time. For time longer than 130 ps, the diffusive regime [Fig. 5(c)], the tails of $G_s(r,t)$ progressively extend in time. We note that only at the lowest temperature and for very long times is there evidence for a very weak double-peak structure of $G_s(r,t)$, suggesting that the hopping contribution to diffusion is negligible in the T range studied.

The almost time-invariant $G_s(r,t)$ in the β region [Fig. 5(b)] contains information on the shape of the confining potential. If we assume that a molecule of mass M is constrained to move in a three-dimensional harmonic potential $M\omega^2 r^2/2$, then the stationary solution for $G_s(r,t)$ is given by

$$G_s(r,t) = \left(\frac{M\omega^2}{4k_B T \pi} \right)^{3/2} e^{-M\omega^2 r^2/4k_B T}, \quad (9)$$

i.e., by a Gaussian distribution. Figure 6 shows that indeed in the time regime between $t=1$ and 8 ps (the center of the β region) $G_s(x,t)$, the one-dimensional analog of $G_s(r,t)$, is rather well represented by a Gaussian distribution in space, corresponding to a confining potential with $\omega = 14.2 \text{ ps}^{-1}$, i.e., with an oscillation period of 0.44 ps. This suggests that the motion of water molecules in the cage at low T has a significant harmonic character. We will return to this point in Sec. IV C.

The intermediate region in which $G_s(r,t)$ is slowly changing in time corresponds to the β -relaxation region described by MCT. In this regime a space-time factorization is

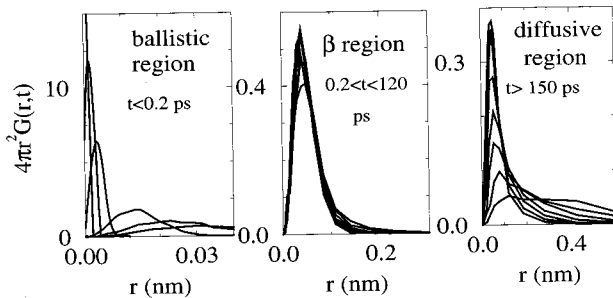


FIG. 5. Self-part of the Van Hove distribution function for the three time regions at the lowest temperature studied: (a) $t < 0.2$ ps, (b) β -relaxation region $0.2 < t < 120$ ps, and (c) α -relaxation region $t > 150$ ps.

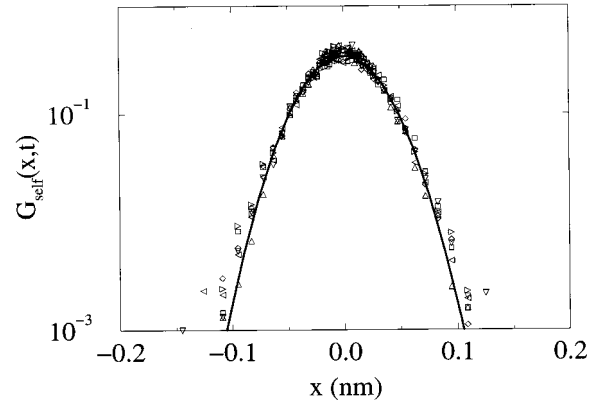


FIG. 6. Symbols, $G_s(x,t)$ for times between 1 ps and 8 ps, full line, Gaussian function with variance 0.00095 nm^2 , describing the behavior of a molecule diffusing in a harmonic potential with $\omega = 14.2 \text{ ps}^{-1}$ (see the text).

supposed to hold [see Eq. (5)]. Figure 7 intends to compare how this prediction of MCT is borne out in our simulated system. In Fig. 7 we show the probability that a molecule has moved less than r during time t , $n(r,t) = \int_0^r 4\pi r'^2 G_s(r',t) dr'$, as a function of time, in the β -relaxation region, for some selected r values. This representation, using the integral of G_s , is less noisy than G_s itself. We show three different r values, corresponding to distances close to and larger than the size of the cage. We expect from Eq. (5) that $n(r,t)$ can be well represented by the functional form $f(r) - g(r)t^b$. From fitting $n(r,t)$ in the β region with such a functional form, we find that the resulting exponent b has an effective value that depends on r . It decreases on decreasing r , in apparent disagreement with MCT. However, if we fit all curves simultaneously with an expansion in terms of t^b up to the second (or third) order, i.e., according to

$$\phi(r,t) \approx f(r) - g(r)t^b + h(r)t^{2b} + \dots, \quad (10)$$

we obtain the single r -independent value $b = 0.50 \pm 0.05$.

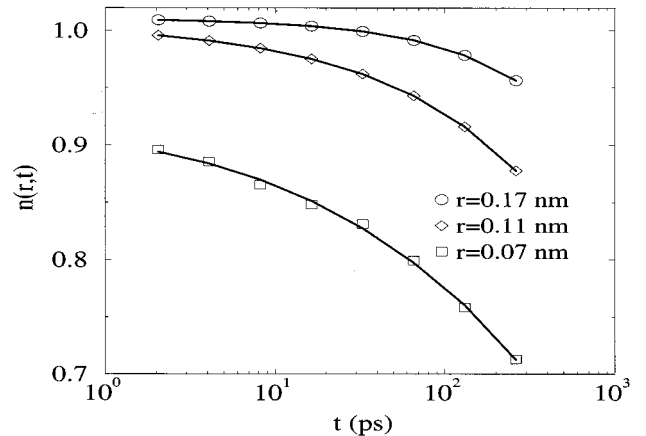


FIG. 7. $n(r,t)$ as a function of time for three selected r values in the β -relaxation region: $r=0.17 \text{ nm}$ (\square), $r=0.11 \text{ nm}$ (\circ), and $r=0.07 \text{ nm}$ (\diamond). Full lines are fit according to a third-order expansion in powers of t^b with $b=0.5$ [see Eq. (10)].

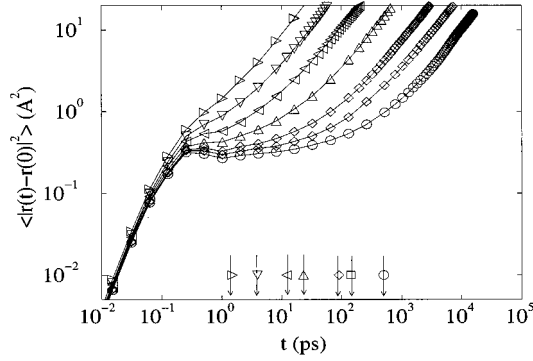


FIG. 8. MSD as a function of time for $T=206.3$ K (\circ), $T=209.3$ K (\square), $T=213.6$ K (\diamond), $T=224.0$ K (\triangle), $T=238.2$ K (\triangleleft), $T=258.5$ K (∇), and $T=284.5$ K (\triangleright). The curves show the cage effect, starting at 0.25 ps, followed by the eventual diffusion of the molecule. Arrows indicate the time at which the non-Gaussian parameter $\alpha_2(t)$ (see the text) is maximum.

We note also in passing that a numerical calculation of $h(r)$ as proposed in Ref. [34] would instead support, within the noise, the validity of Eq. (3). We thus suggest the use of $n(r)$ as the quantity to look at when checking Eq. (3) via simulations. The apparent dependence of the effective b on r will be discussed in more detail in the following.

C. Mean-square displacement and non-Gaussian corrections

We show next the mean-square displacement (MSD) of the oxygen atoms, $\langle r^2(t) \rangle = \langle |\mathbf{r}(t) - \mathbf{r}(0)|^2 \rangle$, for all temperatures studied, in Fig. 8. This is the second spatial moment of $G_s(r, t)$. Curves have been plotted on a log-log scale in order to better display the flattening-out behavior of $\langle r^2 \rangle$ at intermediate times. All curves have an initial t^2 region, describing the ballistic regime. At high T , the ballistic region is followed by the usual diffusive linear dependence in t . However, as already suggested by the behavior of $G_s(r, t)$, for low T an intermediate region develops where $\langle r^2 \rangle$ remains almost flat. Molecules appear to be trapped in a cage for a considerable amount of time before starting to diffuse. Indeed, for the lowest temperature, $\langle r^2 \rangle$ becomes almost flat for three decades in time. During this time, no significant diffusion is present. Molecules vibrate and diffuse mainly within the cage. From the value of $\langle r^2 \rangle$ at the plateau, we estimate the radius of the cage to be about 0.05 nm, very slightly T dependent. Note that the onset of the cage effect appears always at the same time, 0.25 ps, regardless of temperature. This is completely analogous to the corresponding result obtained by Kob and Andersen [15,16] for a binary mixture of Lennard-Jones spheres close to the glass transition. While $\langle r^2 \rangle$ is constant, no significant structural changes happen in the system. Thus, for a long time, the system is frozen in a particular configuration. For longer times, the onset of diffusion allows for structural relaxation.

We note also that at low T , $\langle r^2 \rangle$ shows a small bump for times around 0.35 ps. Such a bump has been tentatively associated with the so-called boson peak [35,19] or with a finite-size effect [15,36]. We recall that in a harmonic solid, even for the simple Debye model with a single Debye frequency $\omega_D = 2\pi/T_D$, $\langle r^2(t) \rangle \sim 1 - \sin(\omega_D t)/\omega_D t$ [37], i.e., it

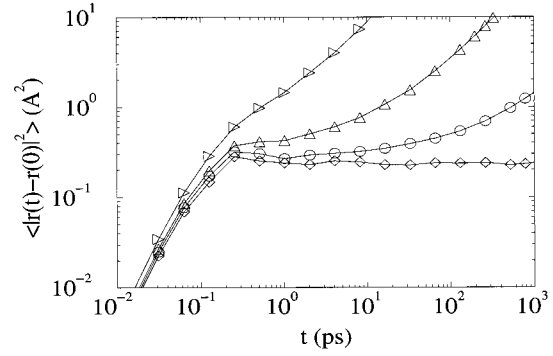


FIG. 9. MSD of oxygen atoms for hexagonal ice and liquid water. \triangleright represent the liquid at $T=284.5$ K, \triangle the liquid at $T=224.0$ K, \circ the liquid at $T=206.3$ K, and \diamond ice at $T=194$ K. The line is a guide for the eyes.

shows an overshoot at $t = 4.49/\omega_D = 0.71T_D$. Thus, using such a simple model for the distribution of modes one obtains $T_D = 0.49$ ps, which is very close to the average period estimated in Sec. IV B from the shape of $G_s(r, t)$ in the β region. We believe that such agreement supports the view that the overshoot in $\langle r^2 \rangle$ is a manifestation of significant quasiharmonic motion in the cage. It would be very valuable to perform a comparative analysis of the presence of an overshoot in $\langle r^2 \rangle$ with the shape of the confining potential, calculated from $G_s(r, t)$, in different systems. If the presence of an overshoot in $\langle r^2 \rangle$ is connected to the molecular harmonic motion in the cage, and if this harmonic motion evidenced in the single-molecule dynamics is the manifestation of a collective harmonic oscillation in the disordered system, then the overshoot of $\langle r^2 \rangle$ could be related to the presence of a significant fraction of harmonic modes. The corresponding signature in frequency may be related to the boson-peak feature, as proposed recently [35]. The study of the collective dynamics of liquid water supported by a normal mode analysis of the corresponding configurations will help in clarifying this important issue.

In Fig. 9 we show the MSD for the oxygen atoms in ice and in the liquid at three selected temperatures. As expected, there is no diffusion for oxygen in ice. It is interesting to observe that there is no substantial difference in the short-time dynamics of water molecules up to 0.25 ps in the liquid and in the solid. The plateau of the MSD of ice starts at a slightly smaller cage of radius of 0.052 nm, as compared to the 0.055 nm at the lowest temperature we studied in the liquid state.

The values of D extracted from the asymptotic behavior of MSD are shown in Fig. 10 together with the fitted curve to the power-law temperature dependence $D = D_0(T/T_c - 1)^\gamma$. We also show the values of D from [30]. For both isobars, the temperature dependence of D is well described by a power law, as in real experiments [38]. T_c and γ are pressure dependent. We find the values 2.7 and 2.3 for γ and 186 and 199 K for T_c for the two isobars. We find that on increasing the pressure, T_c decreases, so that the ideal glass transition line has the same slope in P - T as the TMD and the liquid-ice equilibrium line. The difference between T_c and the corresponding TMD is always about 50 K. We note also that the

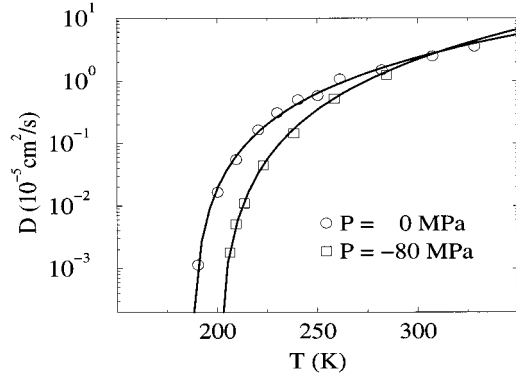


FIG. 10. Temperature dependence of the diffusion coefficient D for two isobars. \square are from Table I and \circ from [30]. Full lines are power-law fits, respectively, given by $D=13.93(T/198.7-1)^{2.73}$ and $D=7.39(T/186.3-1)^{2.29}$, where D is in cm^2/s and T is in K.

difference between T_S and the TMD in real water is also about 50 K. Henceforth, we suggest the possibility of interpreting T_S as the temperature of structural arrest. The differences in γ between the two simulated isobars are consistent with the experimentally observed sensitivity of γ on pressure (see Ref. [38]) and with MCT. Indeed, according to MCT, γ depends on the specific point of the glass transition line $T_c(P)$ approached.

From Fig. 5 we see that $G_s(r,t)$ is apparently a Gaussian function in space only for early times. To quantify the degree of non-Gaussianity we calculate the so-called non-Gaussian parameters $\alpha_n(t)$. $\alpha_n(t)$ are defined by

$$\alpha_n(t) = \frac{3\langle r^{2n}(t) \rangle}{c_n \langle r^2(t) \rangle^n} - 1, \quad c_n = \frac{(2n+1)!!}{3^n}. \quad (11)$$

We note that, as found in several previous simulations of liquids close to the glass transition [36,39], $\alpha_2(t)$ increases significantly in the β region and reaches its maximum when diffusion starts to be significant. For longer times, $\alpha_2(t)$ goes back to zero. This is expected because for long times $G_s(r,t)$ has to go back to a Gaussian shape whose variance is controlled by the diffusion coefficient D . Figure 11 shows the behavior of $\alpha_2(t)$ as a function of T . The time at which $\alpha_2(t)$ is maximum $t_{\alpha_{\max}}$ is also indicated by arrows in Fig. 8. We note that in the case of SPC/E water, $\alpha_2(t)$ increases significantly in the β region, much more than it was observed in some of the previous simulations of supercooled liquids [36,39,40]. The increase in α_2 observed here is comparable to the one calculated for a binary mixture of Lennard-Jones by Kob and Andersen [15]. We also note that $t_{\alpha_{\max}}$ has a power-law dependence on $T-T^*$, as shown in the inset of Fig. 11. The apparent exponent of the T dependence of $t_{\alpha_{\max}}$ is 2.5, which is close to the γ value of 2.7 found in the T dependence of D . A slight change in T^* or the restriction of the T range to the five lowest T would allow a fit of $t_{\alpha_{\max}}$ with an exponent 2.7. $t_{\alpha_{\max}}$ could be used to locate the glass transition [23].

Note that on cooling the system the dynamics becomes more and more nonergodic. The increase of $\alpha_2(t)$ is ob-

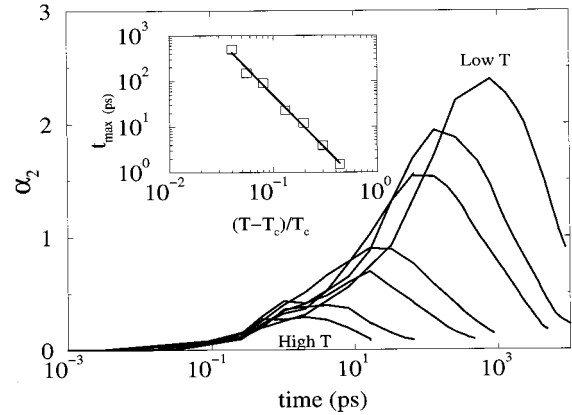


FIG. 11. Non-Gaussian parameter $\alpha_2(t)$ as a function of time for all temperatures studied. The inset shows the T dependence of the position of the maximum $t_{\alpha_{\max}}$ to highlight the power-law dependence on $T/T_c - 1$. The full line is a power law with exponent 2.5.

served in the region where $\langle r^2 \rangle$ is almost flat, suggesting that $t_{\alpha_{\max}}$ could be used to define the β -relaxation region. $\alpha_2(t)$ for the three lowest T is reported in Fig. 12 on a log-log scale. The rise of $\alpha_2(t)$ can well be represented by a power law in time, i.e., $\alpha_2(t) \sim t^{0.4}$, although the small variation of $\alpha_2(t)$ does not allow a definitive conclusion on this point. Analysis of the behavior of $\alpha_2(t)$ for different systems would be very valuable. In particular, it has been proposed that the initial rise of $\alpha_2(t)$ at different T obeys a master curve in time [16]. Data in Fig. 11 support this finding.

To continue testing the space-time decomposition, we study the behavior of $\langle r^n(t) \rangle$ in the β region. $\langle r^n(t) \rangle$ are the n moments of G_s and should thus also follow a von Schweidler law [Eq. (3)] exactly as $G_s(r,t)$. We find that the moments are well described by Eq. (3), with a b exponent that is T independent for all the n th moments of $G_s(r,t)$ with an apparent exponent b varying from 0.7 for $\langle r^2 \rangle$ to 1.1 for $\langle r^4 \rangle$ and 1.4 for $\langle r^6 \rangle$. Because different moments weight different r regions, this finding supports the hypothesis that the apparent b exponent is r dependent. In this case too using

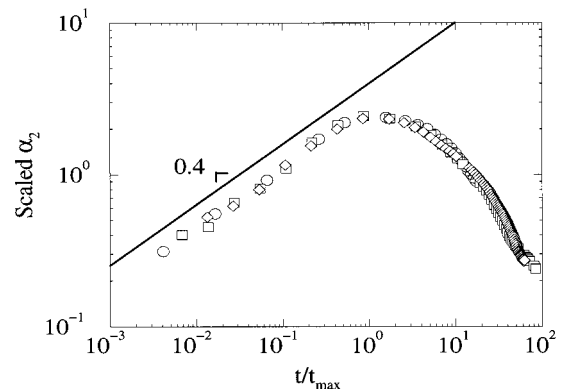


FIG. 12. $\alpha_2(t)$ as a function of t/t_{\max} in log-log scale, for the three lowest T studied. Note the apparent power-law region for $t < t_{\max}$ with slope 0.4.

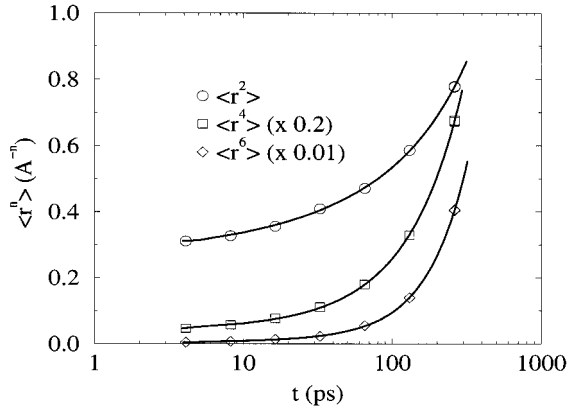


FIG. 13. Behavior of the first three even moments of $G_s(r,t)$ as a function of time in the β region for $T=206.3$ K. Full curves describe a third-order expansion in powers of t^b [see Eq. (10)] with $b=0.5$.

a second- or third-order expansion in t^b as in Eq. (10), we are able to fit simultaneously $\langle r^2 \rangle$, $\langle r^4 \rangle$, and $\langle r^6 \rangle$, with a single value $b=0.50 \pm 0.05$. In Fig. 13 we show $\langle r^2 \rangle$, $\langle r^4 \rangle$, and $\langle r^6 \rangle$ and the best fit for the lowest T .

D. Intermediate scattering function

We now move to the incoherent intermediate scattering function $F_s(Q,t)$, the spatial Fourier transform of the Van Hove self-correlation function $G_s(r,t)$. $F_s(Q,t)$ can be measured by incoherent neutron-scattering experiments. Previous works on the behavior of $F_s(Q,t)$ in simulated water [41–43], although based on a rather limited simulated time scale (up to 10 ps at most) and limited temperature range, have shown that (i) the intermediate scattering function for the center of mass $F_s(Q,t)$ is non-Gaussian except at short times [41], (ii) at room temperature the diffusive behavior of water molecules is not describable by a discrete jump diffusion [41,43], and (iii) the decay of $F_s(Q,t)$ has a fast and a slow component, the time scale of which becomes increasingly disparate upon supercooling [43].

Figure 14 shows the T dependence of $F_s(Q_{\max},t)$. Note

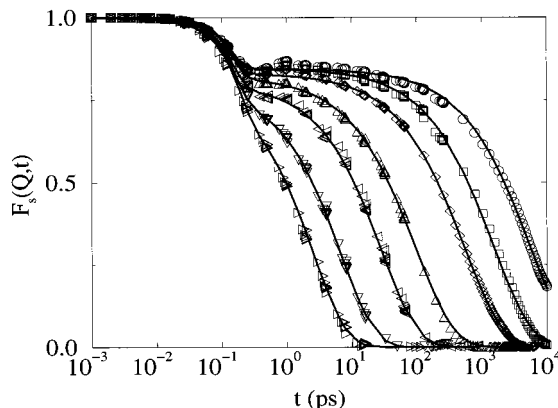


FIG. 14. $F_s(Q_{\max},t)$ vs time (symbols are the same as in Fig. 8). Solid lines are calculated according to Eq. (13).

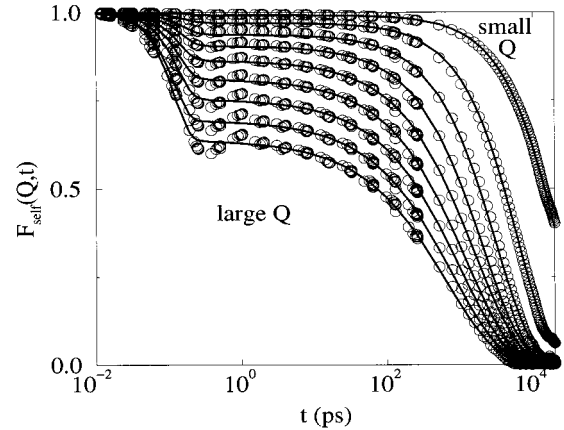


FIG. 15. $F_s(Q,t)$ vs time for different Q values at $T=209.3$ K (from top to bottom, integer multiples of 3.3 nm^{-1}). Solid lines are calculated according to Eq. (13).

that for all T investigated, $F_s(Q_{\max},t)$ decays to zero in the long-time limit. This confirms that the simulations were long enough to guarantee the complete decay to zero of the test particle thermal fluctuations, i.e., that all simulations were in the liquid state and in equilibrium. $F_s(Q_{\max},t)$ also shows the presence of three different regimes, the initial one characterized by a fast decay, followed by a plateau region and by a final decay to zero. Figure 15 shows the Q dependence of $F_s(Q,t)$ at one selected temperature.

For very early times, $F_s(Q,t)$ decays following a quadratic dependence on time, characteristic of the ballistic motion. The initial part of the decay (time shorter than 0.25 ps) is well represented (see below) by

$$F_s(Q,t) = [1 - A(Q)]e^{-(t/\tau_s)^2} + A(Q). \quad (12)$$

This is not surprising because we have seen already that $\alpha_2(r,t)$ is very small in this time range. Moreover, $F_s(Q,t)$, both for ballistic motion and for vibrations in a harmonic potential, is described by a Gaussian function in space [20].

At intermediate times, $F_s(Q,t)$ is slowly varying, confirming the existence of a time region where no significant structural changes are observed. In this time region, molecules have already explored all the space in their cages, but the very slow cage rearrangement prevents the exploration of space outside the cage.

For long times, $F_s(Q,t)$ decays in a nonexponential fashion. We fit the whole curve rather well by the equation

$$F_s(Q,t) = [1 - A(Q)]e^{-(t/\tau_s)^2} + A(Q)e^{-(t/\tau_l)^\beta}, \quad (13)$$

in which the initial decorrelation associated with the motion in the cage is followed by a stretched exponential decay.

Full lines in Figs. 14 and 15 are fit to the data according to Eq. (13). From the fitting procedure we find that τ_s is rather constant and of order 0.15 ps. It has a very weak T dependence as expected. $A(Q)$ is well described by $e^{-a^2 Q^2/3}$, where a is of the order $0.050 \pm 0.003 \text{ nm}$, slightly increasing on increasing T . Figures 16 and 17 show the values obtained

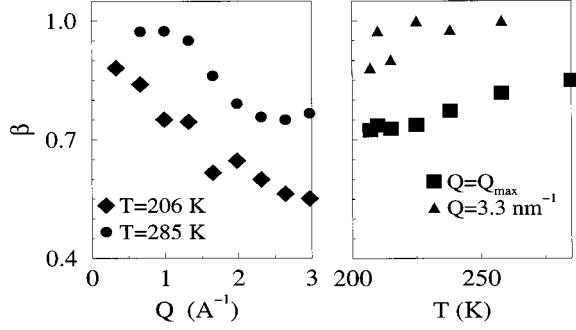


FIG. 16. Results from the fitting procedure for the parameter β . Left panel, β as a function of Q at two different temperatures; right panel, β as a function of T at $Q=Q_{\max}$ and at the smallest available $Q=3.3 \text{ nm}^{-1}$.

from the fit, in both T and Q , for the two most interesting parameters β and τ_l . We note that β starts from 1 at small Q and goes to 0.5 at high Q vectors. There is also a weaker dependence on T , suggesting that β increases on increasing T . This Q and T dependence of β is what one would expect for a phenomenon that happens on a well-defined length scale. When the inverse of the Q vector is much bigger than the cage size, the slow dynamics evidenced by the stretched exponential ceases to be relevant. On large distances, compared to the cage dimension, diffusion is normal and the decay of self-density fluctuations goes back to the usual exponential e^{-DQ^2t} form (i.e., $\beta=1$). Similarly, on increasing the temperature, cages break and reform on a faster rate and the convergence of the stochastic process to a Gaussian is faster. We look next to τ_l . τ_l indicates the time it takes for a self-density fluctuation to die out over length of Q^{-1} , i.e., the time it takes a molecule to diffuse over distances of order Q^{-1} . For large distances and all T , the leading propagation mechanism is diffusion, which implies that $\tau_l=(DQ^2)^{-1}$. For small distances, at high T , we still observe the Q^2 behavior, in agreement with the fact that $\alpha_2(t)$ is not very large. From Fig. 17 we observe that $\tau_l DQ^2=1$ at low Q and high T , while at high Q and low T significant deviations are

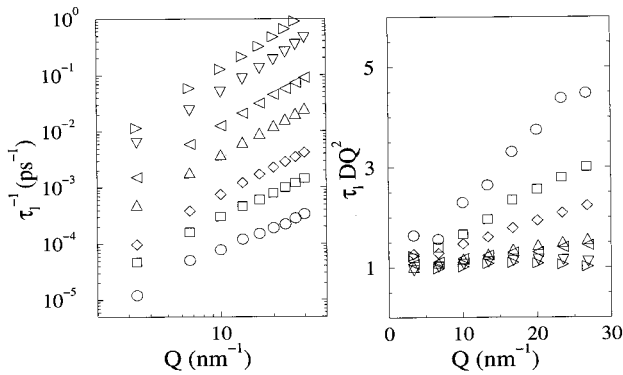


FIG. 17. Results from the fitting procedure for the parameter τ_l . The left panel shows the Q dependence of τ_l at all temperatures (symbols are the same as in Fig. 8). The right panel shows $DQ^2\tau_l$ as a function of Q . Note that at low T and high Q , $DQ^2\tau_l$ increases linearly, suggesting that $\tau_l \sim Q^{-1}$.

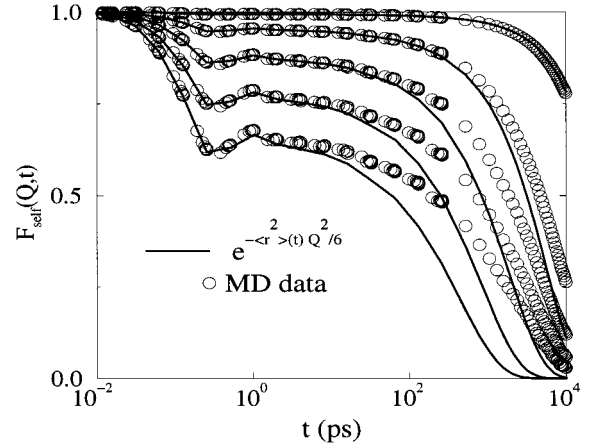


FIG. 18. Comparison between the time dependence of $F_s(Q,t)$ and the Gaussian approximation $e^{-Q^2\langle r^2(t)\rangle/6}$ at $T=206.3 \text{ K}$, for Q equal to odd multiples of 3.3 nm^{-1} . Note how the Gaussian approximation is worse on increasing Q .

present. τ_l^{-1} seems to cross from a Q^2 to a Q behavior. Note that a Q^2 dependence has been observed for glycerol close to its glass transition [44]. At low T , τ_l is bigger than one would expect if diffusion were the only mechanism. This suggests that on short length scales diffusion is slower than it would be, suggesting the presence of anomalous diffusion over small scales. It should be noted that we do not find $\tau_l \sim Q^{-2/\beta}$ at large Q and small T , as was observed, e.g., in glass forming microemulsions and polymer melts [45,46]. This difference probably stresses the highly non-Gaussian behavior of the dynamics in SPC/E water. Indeed, the behavior $\tau_l \sim Q^{-2/\delta}$ is expected when $G_s(r,t)$ is a Gaussian in space with a variance growing as t^δ .

To complete the picture of self-motion in water, we discuss the role of the non-Gaussianity in the decay of $F_s(Q,t)$, which can be formally expanded as [20]

$$F_s(Q,t) = e^{-Q^2\rho_1(t)} \left[1 + \frac{1}{2!} \alpha_2(t) [Q^2\rho_1(t)]^2 - \frac{1}{3!} [\alpha_3(t) - 3\alpha_2(t)] [Q^2\rho_1(t)]^3 + \dots \right], \quad (14)$$

where $\rho_1(t) = \langle r(t)^2 \rangle / 6$ and α_n are given in Eq. (11). In Eq. (14) the leading term is a Gaussian function in Q . The leading term at different Q vectors is shown in Fig. 18 and compared with the actual $F_s(Q,t)$. As discussed above, we see that the Gaussian approximation represents the data well at small Q for all times. At larger Q the decay deviates more and more from the Gaussian behavior, starting from the β region. In Fig. 19 we show the first four approximations in the expansion of Eq. (14). We note that the convergence is very slow and nonmonotonic, preventing the possibility of measuring unambiguously $\alpha_2(t)$ from the Q dependence of $F_s(Q,t)$ [23].

We also note that the bump in $F_s(Q,t)$ observed around 1 ps comes from the presence of a minimum in $\langle r^2(t) \rangle$ at the same time. Oscillations in $\langle r^2(t) \rangle$ are thus responsible for the oscillations observed in $F_s(Q,t)$. A bump in $F_s(Q,t)$ was

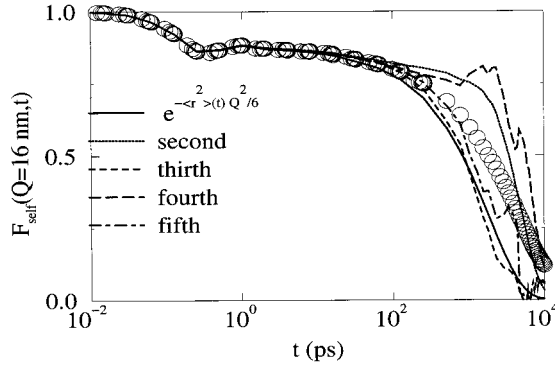


FIG. 19. Comparison between $F_s(16 \text{ nm}^{-1}, t)$ and the first four approximations in the expansion of Eq. (14) at $T=206.3 \text{ K}$.

observed in recent simulations of orthophenil [36], Lennard-Jones [15], and others deeply supercooled liquids [47,34]. As discussed in Secs. IV B and IV C, we attribute oscillation in $F_s(Q, t)$ to the almost harmonic motion of molecules in the cages.

We now come to a more detailed study of the behavior of the correlator $F_s(Q, t)$ in the late β region. As discussed in Sec. II, all correlators are supposed to decay as a power law with the von Schweidler exponent b [Eq. (3)]. Figure 20 shows that, for all low temperatures such that a β region is clearly established, the fit with a power law is superior to the stretched exponential form. The Q dependence of b is instead at odds with the predictions of MCT. We find that the apparent exponent b , as calculated from fitting the time dependence of $F_s(Q, t)$ in the β region, apparently decreases on increasing Q . It goes from the value 0.7 at the smallest Q down to about 0.3 at high Q . At Q_{\max} the value of the effective b consistently is given by $b=0.50 \pm 0.05$. Again, using a three-term expansion, a simultaneous fit of all curves gives a single value $b=0.50 \pm 0.05$, independent on Q , as shown in Fig. 21. The decrease of the apparent b on decreasing Q was also detected in a previous calculation of Lennard-Jones mixtures close to the glass transition [15].

As discussed in Sec. II, the exponents b and γ are related by MCT. We measure independently both exponents, one

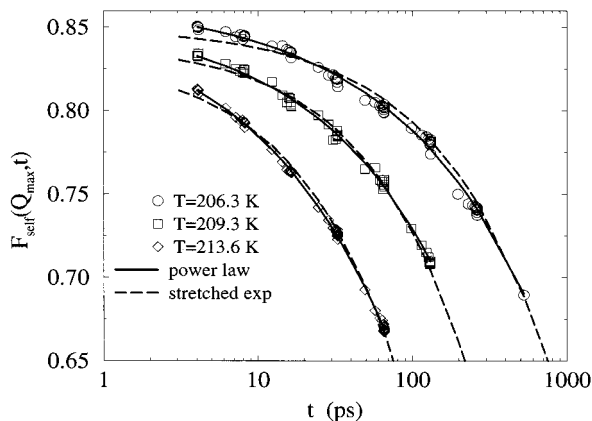


FIG. 20. Comparison between the stretched exponential and the von Schweidler law in the β region. Full curves are compared with $F_s(Q_{\max}, t)$ at the three lowest temperatures.

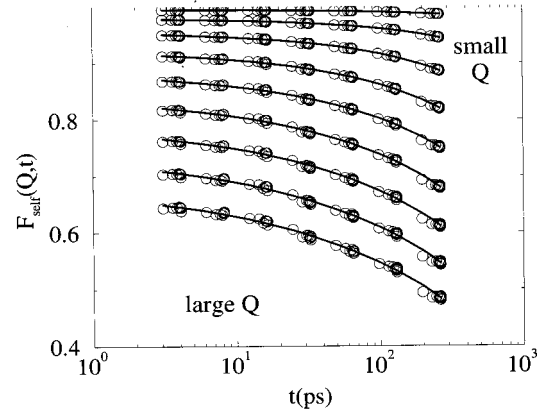


FIG. 21. Fit in the late β region of $F_s(Q, t)$ for different Q values (from top to bottom, integer multiples of 3.3 nm^{-1}) for the smallest temperature studied. Lines are a simultaneous fit to all curves according to a third-order expansion of $F_s(Q, t)$ in powers of t^b [see Eq. (10)] with $b=0.5$.

from the t dependence of the correlators in the β region and one from the T dependence of D . The resulting (b, γ) pair obtained for SPC/E water is shown in Fig. 1. The agreement between our calculated value and the theory is surprisingly good. We note in passing that the value of b calculated from a third-order fit in power of t^b of the time dependence of several correlators in the late β region coincides with the apparent b obtained by fitting according to the von Schweidler law when $Q=Q_{\max}$. The choice of the value of b at Q_{\max} in comparing the MCT relation Eq. (6) and the numerical or experimental results often has been assumed implicitly in several previous studies.

E. Rotational dynamics

In the previous subsections we have presented the translational properties looking at the motion of the oxygen atoms, very close to that of the center of mass of a water molecule. In this subsection we analyze some aspects of rotational motions of the molecule. We focus our attention on the motion of the dipole vector $\boldsymbol{\mu}$, i.e., on the time evolution of the angle $\theta(t) = \cos^{-1}[\langle \boldsymbol{\mu}(t) \cdot \boldsymbol{\mu}(0) \rangle / \langle \boldsymbol{\mu}(0) \cdot \boldsymbol{\mu}(0) \rangle]$. The first two angular correlation functions

$$C_l(t) = \langle P_l[\cos\theta(t)] \rangle, \quad (15)$$

where P_l is the l -order Legendre polynomial, are experimentally measurable quantities. In particular, $C_1(t)$ can be measured by dielectric relaxation experiments and $C_2(t)$ can be measured by NMR.

The time evolution of $C_l(t)$ for supercooled SPC/E water shows also a two-step relaxation scenario. The initial relaxation ($t < 1 \text{ ps}$) is modulated by the librational motion of the water molecules. The initial decay is followed at low T by a plateau region and in the end by the α relaxation decay. Figures 22 and 23 show the behavior of $C_1(t)$ and $C_2(t)$ as a function of time for all T . We find that the slow relaxation can be well described by a stretched exponential decay. The exponent β increases on increasing temperature. The results of the fit to a stretched exponential behavior for $t > 1 \text{ ps}$ are

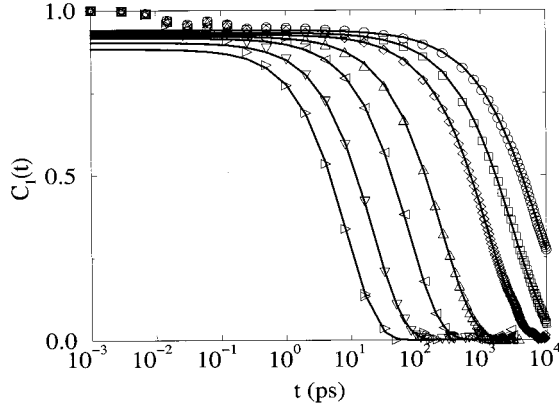


FIG. 22. Dipole moment autocorrelation function $C_1(t)$ as a function of time for all T studied (symbols are the same as in Fig. 8). Full lines are fit to a stretched exponential form, for $t > 1$ ps. Fitting parameters are given in Table II.

reported in Table II. We note that the decay time of $C_1(t)$ is close to the decay time of $F(Q_{\max}, t)$. This suggests that angular decorrelation happens on the same time scale of diffusion over distances of the order Q_{\max}^{-1} i.e., over nearest-neighbor distances. The breaking and reforming of cages is the bottleneck for both rotational and translational diffusion. The fact that $C_1(t)$ follows the same pattern as $F_s(Q, t)$ suggests also that molecules in cages perform hindered rotations (librations). Rotations within the cage would indeed require the breaking of at least three hydrogen bonds, which, due to the HB strength, is a process with a very low probability [31].

V. DISCUSSION AND CONCLUSIONS

We have presented evidence that SPC/E water undergoes a kinetic glass transition 50° below the TMD. The molecular dynamics is well accounted for by the idealized MCT of supercooled liquids, suggesting an interpretation of the so-called Angell temperature as the critical temperature of MCT

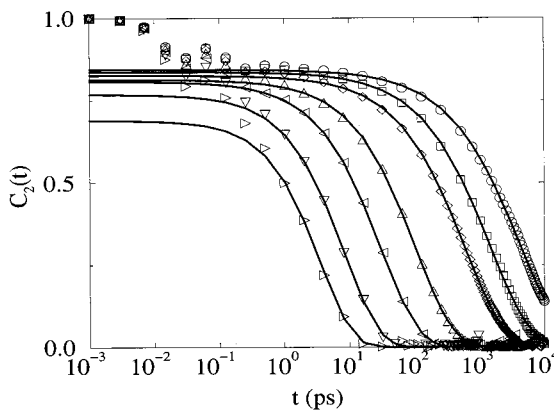


FIG. 23. Dipole moment autocorrelation function $C_2(t)$ as a function of time for all T studied (symbols are the same as in Fig. 8). Full lines are fit to a stretched exponential form, for $t > 1$ ps. Fitting parameters are given in Table II.

TABLE II. Stretched exponential ($Ae^{-(t/\tau)^\beta}$) fitting parameters of the dipole moment autocorrelation functions $C_1(t)$ and $C_2(t)$.

T (K)	A	β	τ (ps)
$C_1(t)$			
284.5	0.884	0.957	0.851×10^1
258.5	0.903	0.918	0.216×10^2
238.2	0.916	0.907	0.745×10^2
224.0	0.922	0.877	0.243×10^3
213.6	0.928	0.841	0.122×10^4
209.3	0.933	0.816	0.298×10^4
206.3	0.941	0.776	0.755×10^4
$C_2(t)$			
284.5	0.690	0.904	0.364×10^1
258.5	0.769	0.826	0.853×10^1
238.2	0.808	0.763	0.311×10^2
224.0	0.814	0.755	0.106×10^3
213.6	0.827	0.714	0.597×10^3
209.3	0.838	0.702	0.146×10^4
206.3	0.845	0.677	0.425×10^4

[17]. In this regard, the apparent power-law increase of the transport coefficient in liquid water on supercooling is traced to the formation of cages and to the associated slow dynamics resulting from the presence of long-lived cages. In other words, the divergence of transport coefficients does not need to rely on a thermodynamical instability, either connected to the reentrance of the gas-liquid spinodal or to the presence of a critical point at high pressure and low temperature. The SPC/E behavior described in this work thus supports the recently presented thermodynamic analysis of liquids with a negatively sloped TMD in the absence of singularities [9].

It is important at this point to stress that the finding of this work could easily be tested by performing QENS experiments. Indeed we found that the detailed shape of the slow relaxation part of the $F_s(Q, t)$ can be described very accurately by a stretched exponential decay around and above Q_{\max} . It is remarkable to observe that at Q_{\max} the slow relaxation is already clearly visible at 12° below the TMD, which is easily realizable in a QENS experiment of bulk water. Unfortunately, in a previous QENS experiment of supercooled bulk water the instrumental resolution used was 84μ eV, which did not allow one to clearly see the line shape characteristic of the stretched exponential relaxation (a Cole-Cole dispersion function) [48]. The T dependence of β at Q_{\max} can also be tested, as well as the Q dependence of τ_l and its crossing from a Q^2 behavior at small Q to a Q behavior at high Q at low T .

The scenario described above bears a strong resemblance to the results of MD simulation for the mixed Lennard-Jones spheres carried out recently to test the MCT of kinetic glass transition. In this respect, the prediction of the idealized MCT seems to be robust, and able to describe fragile liquids [49], for molecules interacting via spherical as well as highly directional potentials. It is indeed surprising that a simple Lennard-Jones system, in which molecules are confined in cages with a large coordination number, behaves, close to its glass transition, similarly to a tetrahedrally coordinated system, like SPC/E water, in which the cages are formed more

by the deep hydrogen-bonding potential than by the excluded-volume constraint.

The dynamics in SPC/E water is seen to be characterized by (i) a fast and a slow relaxation process, (ii) the presence of a time region in which dynamics is self-similar in time. [In this region, correlations decay as a power law whose range of validity is r dependent. The range of validity of the von Schweidler law is maximum for distances close to the first neighbors shell or Q values close to the maximum of the $S(Q)$], (iii) a late-time region where $C(t)$ decays as a stretched exponential (the value of the stretching exponent β is T and Q dependent), and (iv) the divergence of the small- Q relaxation times as a power law in T with an exponent γ that is the same as that of the diffusion coefficient. Furthermore, the relation between γ and the exponent b , calculated in the self-similar β -relaxation region, is in agreement with MCT predictions.

As noted in Ref. [44], points (i)–(iii) by themselves are not sufficient for validating MCT. Glycerol has indeed a two-step relaxation, characterized by a T -independent short-time decay followed by a stretched exponential decay, but relations between γ and b are clearly not fulfilled. We thus consider particularly interesting the finding of point (iv).

The picture we get from this study is that the system goes back to a “normal” behavior for distances much bigger than the cage size. Indeed, we find that for small Q , the stretched exponential behavior tends to the usual simple exponential behavior, diffusion becomes normal, τ_l^{-1} scales as Q^2 , and the Gaussian approximation for $F_s(Q, t)$ becomes sufficiently good to represent the data. At a small- Q vector, the presence of a nearby ideal glass transition appears only via the T dependence of D and τ_l .

Studying the shape of the self-Van Hove correlation function in the β region, we have found that molecules undergo harmonic motion within the cage or, in other words, the shape of the confining potential is significantly harmonic. We have shown that such harmonic motion manifests itself in an overshoot in $\langle r^2(t) \rangle$ and in oscillations in $F_s(Q, t)$ for early times ($t < 1 \sim 3$ ps). In this regime, the dynamics is significantly Gaussian, as expected for ballistic motion, harmonic oscillations, and diffusion in a harmonic potential [37]. This kind of analysis may offer a way of testing the proposed relation between the effective shape of the cage potential and the so-called boson peak [35].

We also note that the system studied in the present work is composed of only 216 water molecules; the larger system we managed to study due to the very long simulation needed to equilibrate the system and to produce uncorrelated events.

A size-dependent study would be very valuable. This notwithstanding, we would like to stress that even such a small system shows all the characteristics predicted by MCT, as discussed in the previous sections. In particular, the β -relaxation region is very clearly observable. All the quantities studied show the predicted power-law behavior in time. Thus, even such a small system is able to generate the self-similar dynamics characteristic of the β region. This could suggest that the relevant length scale in the glass transition phenomenon does not extend beyond one or two coordination shells, at least for water.

Before concluding we wish to review the results of a recent MD study on single-particle diffusion in water [50] performed using the ST2 model potential. The studied region is the $P = 80$ MPa isochore for T between 250 and 350 K (corresponding to densities $0.87\text{--}1.0$ g/cm³). Along such an isochore, the TMD is 310 ± 10 K. For T larger than 260 K (again 50 K below the TMD) the diffusion process was found to be continuous, but controlled by hopping below 260 K. In the ST2 model, at low T , D follow an Arrhenius law, with an activation energy of about 115 kJ/mol, a value close to the breaking of four hydrogen bands. Above $T = 260$ K, D seems to increase almost linearly with T . It is well known that the ST2 potential gives a much more structured liquid than SPC/E, so that similar structural and thermodynamic quantities are observed by *shifting* the state point by more than 50 K [7]. One possible explanation of such a difference is that when cages start to form in ST2, kT is still large enough to activate a significant fraction of molecular jumps, preventing the possibility of observing the approach of the kinetic glass transition, and to observe both the power-law behavior of D and the stretched exponential decay of $F_s(Q, t)$. Indeed, at $T = 260$ K, where dynamics change in ST2, D is rather large (0.1×10^{-c} cm²/s). If this is the case, a detailed comparative study of the dynamics in these two models could shed light on the origin in the differences between strong and fragile liquids [49] and on the proposed transition between these two behaviors on supercooling water [51].

ACKNOWLEDGMENTS

P.G. acknowledges financial support from the Foundation Blancflor Boncompagni-Ludovisi. The research of S.-H.C. is funded by the U.S. Department of Energy. The research of F.S. and P.T. is supported by GNSM/CNR and INFM/MURST. F.S. thanks C.A. Angell, W. Kob, W. Götze, and R. N. Mantegna for useful discussions and/or comments on the manuscript.

-
- [1] C. A. Angell, *Annu. Rev. Phys. Chem.* **34**, 593 (1983).
 [2] C. A. Angell, in *Water: A Comprehensive Treatise*, edited by F. Franks (Plenum, New York, 1981), Chap. 1.
 [3] P. G. Debenedetti, *Metastable Liquids* (Princeton University Press, Princeton, in press).
 [4] R. J. Speedy, *J. Chem. Phys.* **86**, 982 (1982).
 [5] R. J. Speedy and C. A. Angell, *J. Chem. Phys.* **65**, 851 (1976).
 [6] P. H. Poole, F. Sciortino, T. Grande, H. E. Stanley, and C. A.

- Angell, *Phys. Rev. Lett.* **73**, 1632 (1994).
 [7] P. H. Poole, F. Sciortino, U. Essmann, and H. E. Stanley, *Nature* **360**, 324 (1992).
 [8] H. E. Stanley and J. Teixeira, *J. Chem. Phys.* **73**, 3404 (1980).
 [9] S. Sastry, P. G. Debenedetti, F. Sciortino, and H. E. Stanley, *Phys. Rev. E* **53**, 6144 (1996).
 [10] F. X. Prielmeir, E. W. Lang, R. J. Speedy, and H. D. Lüdemann, *Phys. Rev. Lett.* **59**, 1128 (1987).

- [11] C. A. Angell, *Nature* **331**, 206 (1988).
- [12] E. Leutheusser, *Phys. Rev. A* **29**, 2765 (1984); U. Bengtzelius, W. Götze, and A. Sjölander, *J. Phys. C* **17**, 5915 (1984).
- [13] A. P. Sokolov, J. Hurst, and D. Quitmann, *Phys. Rev. B* **51**, 12 865 (1995).
- [14] W. Götze and L. Sjögren, *Rep. Prog. Phys.* **55**, 241 (1992).
- [15] W. Kob and H. C. Andersen, *Phys. Rev. E* **51**, 4626 (1995); **52**, 4134 (1995).
- [16] *Annu. Rev. Comput. Phys.* **3**, 1 (1996).
- [17] P. Gallo, F. Sciortino, P. Tartaglia, and S. H. Chen, *Phys. Rev. Lett.* **76**, 2730 (1996).
- [18] K. Kawasaki, *Transp. Theory Stat. Phys.* **24**, 755 (1995).
- [19] W. Götze and L. Sjögren, *Chem. Phys.* **XX** (X) (1996), special issue on rate processes with kinetic parameters distributed in time and space, edited by Y. A. Berlin, J. R. Miller, and A. Plonka.
- [20] J. P. Boon and S. Yip, *Molecular Hydrodynamics* (McGraw-Hill, New York, 1980).
- [21] M. Fuchs, I. Hofacker, and L. Latz, *Phys. Rev. A* **45**, 898 (1992).
- [22] W. Götze and A. Sjögren, *Transp. Theory Stat. Phys.* **24**, 801 (1995).
- [23] T. Odagaki and Y. Hiwatari, *Phys. Rev. A* **43**, 1103 (1991); *ibid.* **41**, 929 (1990); T. Odagaki, J. Matsui, and Y. Hiwatari, *Phys. Rev. E* **49**, 3150 (1994).
- [24] T. Odagaki, *Phys. Rev. Lett.* **75**, 3701 (1995).
- [25] H. J. C. Berendsen, J. R. Grigera, and T. P. Straatsma, *J. Phys. Chem.* **91**, 6269 (1987).
- [26] O. Steinhauser, *Mol. Phys.* **45**, 335 (1982).
- [27] P. H. Poole, F. Sciortino, U. Essmann, and H. E. Stanley, *Phys. Rev. E* **48**, 3799 (1993).
- [28] H. J. C. Berendsen *et al.*, *J. Chem. Phys.* **81**, 3684 (1984). The thermostat time constant has been set to 200 ps to compensate the very small energy drift produced by the numerical integration. The very long simulations presented in this work could not be performed in a *pure* constant energy ensemble.
- [29] Y. Guissani and B. Guillot, *J. Chem. Phys.* **98**, 8221 (1993); P. E. Smith and W. F. van Gusteren, *Chem. Phys. Lett.* **215**, 315 (1993).
- [30] L. A. Baez and P. Clancy, *J. Chem. Phys.* **101**, 9837 (1994).
- [31] F. Sciortino, A. Geiger, and H. E. Stanley, *J. Chem. Phys.* **96**, 3857 (1990).
- [32] I. Vaisman, L. Perera, and M. L. Berkowitz, *J. Chem. Phys.* **98**, 9859 (1993).
- [33] A. H. Narten and H. A. Levy, *J. Chem. Phys.* **55**, 2263 (1971).
- [34] G. F. Signorini, J. L. Barrat, and M. Klein, *J. Chem. Phys.* **92**, 1294 (1990).
- [35] C. A. Angell, *Science* **267**, 1924 (1995).
- [36] L. J. Lewis, *Phys. Rev. E* **50**, 3865 (1994).
- [37] G. H. Vineyard, *Phys. Rev.* **110A**, 999 (1958).
- [38] E. W. Lang and H. D. Lüdemann, *Angew. Chem. Int. Ed. Engl.* **21**, 315 (1982).
- [39] B. Bernu, J. P. Hansen, Y. Hiwatari, and G. Pastore, *Phys. Rev. A* **36**, 4891 (1987).
- [40] J. P. Hansen and S. Yip, *Transp. Theory Stat. Phys.* **24**, 1149 (1995).
- [41] A. Rahman and F. H. Stillinger, *J. Chem. Phys.* **55**, 3336 (1971); F. H. Stillinger and A. Rahman, *ibid.*, **57**, 1281 (1972); *Molecular Motions in Liquids*, edited by J. Lascombe (Reidel, Dordrecht, 1974), p. 479.
- [42] R. W. Impey, P. A. Madden, and I. R. McDonald, *Mol. Phys.* **46**, 513 (1982).
- [43] J. J. Ullo, *Phys. Rev. A* **36**, 816 (1987).
- [44] W. Petry and J. Wuttke, *Transp. Theory Stat. Phys.* **24**, 1075 (1995).
- [45] E. Y. Sheu, S. H. Chen, J. S. Huang, and J. C. Sung, *Phys. Rev. E* **39**, 5867 (1989).
- [46] J. Colmenero, A. Alegria, A. Arbe, and B. Frick, *Phys. Rev. Lett.* **69**, 478 (1992).
- [47] H. Löwen, J. P. Hansen, and J. N. Roux, *Phys. Rev. A* **44**, 1169 (1991).
- [48] J. Teixeira, M. C. Bellissant-Funel, S. H. Chen, and A. Dianoux, *Phys. Rev. A* **31**, 1913 (1985).
- [49] C. A. Angell, in *Relaxations in Complex Systems*, edited by K. Ngai and G. B. Wright (National Technical Information Service, U.S. Department of Commerce, Springfield, VA, 1985), p. 1; C. A. Angell, *J. Chem. Phys. Solids* **49**, 863 (1988).
- [50] D. Paschek and A. Geiger (unpublished).
- [51] C. A. Angell, *J. Phys. Chem.* **97**, 6339 (1993).